Whole-body Control with Disturbance Rejection through a Momentum-based Observer for Quadruped Robots

Viviana Morlando[a,*], Ainoor Teimoorzadeh[b], Fabio Ruggiero[a]

[a] *PRISMA Lab, Department of Electrical Engineering and Information Technology, University of Naples Federico II, Via Claudio 21, 80125, Naples, Italy.*
[b] *Department of Electrical Engineering, Sahand University of Technology, Tabriz, Iran.*

Abstract

This paper presents an estimator of external disturbances for legged robots, based on the system's momentum. The estimator, along with a suitable motion planner for the trajectory of the robot's center of mass and an optimization problem based on the modulation of ground reaction forces, devises a whole-body controller for the robot. The designed solution is tested on a quadruped robot within a dynamic simulation environment. The quadruped is stressed by external disturbances acting on stance and swing legs indifferently. The proposed approach is also evaluated through a comparison with two state-of-the-art solutions.

Keywords: Whole-body control, Momentum-based estimator, Quadruped robots

Supplementary Material

Video is available at: `https://www.youtube.com/watch?v=styHnKxOot8`.
Code can be found at: `https://github.com/prisma-lab/WBC_quadruped_DOB`.

1. Introduction

The main advantage of legged robots is the capability to move through complicated and challenging terrains. Thus, they are expected to start collaborating with humans in daily life tasks and being an essential resource in dangerous situations like search and rescue after environmental disasters.

In recent years, research has focused on realizing highly dynamic gaits and improving the ability to maintain a stable balance during the motion to recreate the natural movement of living beings. Despite the significant advances made in motion planning and control methods, legged robots cannot yet cope with all the difficulties of unstructured environments. Since this kind of robots have started to be recently used in tasks such as inspection or patrolling, where the environment is confined or cluttered, the robot needs not only to retain its balance and adapt its foothold to the slope and the roughness of the terrain but also to reject external disturbances.

A powerful tool for robust control and disturbance rejection is the momentum-based observer due to its simple structure and high performance. This kind of observer can handle external forces acting on the robot through the dynamic model. For this reason, a momentum-based observer for a quadruped robot is presented in this paper. Given the inputs from a suitable motion planner, the observer's estimation is combined with a quadratic programming (QP) devising a whole-body controller based on the decoupling of the centroidal's dynamics (i.e., the dynamics of the center of mass) from the legs' ones.

⋆The research leading to these results has been supported by both the PRINBOT project (in the frame of the PRIN 2017 research program, grant number 20172HHNK5_002) and the WELDON project (in the frame of Programme STAR, financially supported by UniNA and Compagnia di San Paolo). The authors are solely responsible for its content.

*Corresponding author
Email address: `viviana.morlando@unina.it` (Viviana Morlando)

When the robot works in a situation where the surface's roughness represents the only external disturbance, the assumption that these unknown forces act only on the support legs can be made. In that case, from a computational viewpoint, it is more convenient to estimate only the external wrench acting on the center of mass [1, 2, 3]. However, the whole-body controller presented in this paper, similarly to [4], works in those situations where the assumption that the unknown external wrench acts only on the support legs cannot be made. Hence, the disturbances may also act on swing legs, as in severe atmosphere conditions or in cluttered spaces where it is easy to have a collision between a moving leg and the environment. During the walking of a legged robot, it is crucial to guarantee good tracking of the center of mass trajectory to retain the balance. When a leg is pushed or subject to a collision, there is also the need to minimize foot drifting, which could bring a loss of balance. The controller here presented demonstrated to perform a good tracking of both center of mass and feet position.

The paper is organized as follows. The related work and the provided contributions are presented in the next section. The dynamic model of the quadruped is presented in Section 3, where the proposed momentum-based observer is detailed. Instead, Section 4 presents the whole-body controller. The platform used for the dynamic simulations, six case studies, and a critical discussion are described in Section 5. Conclusions and future work are finally provided in Section 6.

2. Related Work

Research in legged robotics focuses on realizing control frameworks that could guarantee stable motions. An open challenge regards highly dynamic gaits for biped robots, which have an inherently unstable structure. The same instability characterizes quadruped robots when moving at least two legs (i.e., trot, pace, or gallop). For this reason, locomotion controllers for biped robots are usually adapted for quadrupeds. A common approach for quadrupedal locomotion control is to exploit a reduced model, representing the quadruped as a biped robot [5] or as a cart-table. Standard controllers, like those for a linear inverted pendulum, can be employed to exploit these reduced models [6]. Although these approximations reduce the design complexity and the computation overhead, they could limit dynamism. To avoid this situation, most controllers usually take into account the full dynamic of the robot.

A widely used approach, based on the full dynamic of the robot, employs operational-space control. The desired motion is imposed for relevant points, such as the center of mass or a reference point for feet and hands. This approach found wide application both for biped and quadruped robots [7, 8, 9, 10, 11]. The framework usually exploits the inverse dynamics imposing various priorities for different tasks. The task with higher priority always regards the equation of motion guaranteeing dynamic consistency, while secondary tasks can track a desired motion, force, or torque. Techniques based on null space projection or a standard constrained QP ensure that priorities are respected.

The QP methodology is often used in legged robotics, such as in [12], where a zero moment point (ZMP)-based optimization problem is solved to find optimal joint torques and accelerations that guarantee the tracking of the previously generated trajectory. Since there is no modulation of the ground reaction forces, this control was modified in [13, 14] to find optimal joint accelerations and contact forces, obtaining better results in terms of robustness. A similar approach was presented in [2] with the assumption of a quasi-static dynamic and without achieving highly dynamic gaits. Another approach, still considering the full dynamic, is the model predictive control, which can stabilize the robot by predicting the movements over a finite horizon. Given the nonlinearity of the legged robots dynamic, sometimes, a nonlinear predictive optimization is used instead [15, 16, 17, 18]. All these controllers based on whole-body dynamics decouple the motion planning from the control. There is often the possibility of online re-planning, which contributes to coping with the roughness of the terrain and all the external disturbances.

The robustness against external disturbances has been widely investigated across the years for both quadruped and biped robots. Most of the studies concentrated on the external forces given by the touchdown phase of the feet. This because one of the main capabilities of a legged robot is to traverse challenging terrain. Indeed, given its irregularity, the foot could have an anticipated impact on the ground, causing external forces acting on the system [19, 20]. A solution to this problem is provided in [21], where an impedance control approach using contact forces is performed to obtain references for feet. This kind of impedance controller has also been used for quadrupeds in [9], adding an impedance estimation of external forces on swing legs.

In some cases, these disturbances are taken into account with the use of an observer. In [22], a momentum-based observer detects the anticipated touchdown of the foot, sending this information to a framework of Kalman

filtering to increase robustness. A disturbance observer model for floating base robots using kinematic constraints on fixed contact positions, such as the supporting foot, is proposed in [23]. In most cases, the observer's estimation is integrated into an algorithm acting on the center of mass, and the only disturbances taken into consideration are those applied to it [1, 2, 23, 3], assuming no external force on swing legs. For example, a nonlinear disturbance observer is presented in [4, 24] as a virtual force sensor, and it is applied in combination with sliding control. In this case, coupling forces between the legs and the torso of the robot are estimated. However, it is assumed that there is no disturbance on the swing leg.

Using an observer for external wrenches acting only on the center of mass can robustify the locomotion on uneven terrains. However, it does not prevent the robot from falling after a severe impact on the swing leg. Indeed, this collision causes a drift of the foot from the desired motion so that the touchdown could happen far away from the planned foothold, reducing the support polygon and unbalancing the robot. In worst cases, the swing leg may not touch the ground or may impact against another leg, making the robot fall. For this reason, it is necessary to estimate external forces acting on swing legs and compensate for the disturbance. An estimation of the external forces through impedance control on swing legs has been carried out in [9]. However, such a methodology is not integrated with an observer, and it is used only for static or quasi-static situations.

With respect to the literature review depicted above, this paper aims to estimate disturbances for both stance and swing legs, devising a whole-body controller that, integrating such estimation, allows the execution of dynamic gaits.

2.1. Contributions

The work presented in this paper falls inside the category of whole-body controllers applied for a quadruped robot. It consists of a suitable motion planner that is decoupled from the controller. This last is composed of a QP process working together with an observer based on the system's momentum. As evident from the state of the art above, the overall approach is not new within the community. Nevertheless, compared to existing approaches, the proposed observer and how it is applied with respect to the system's dynamics create an appealing framework for improving the robot's robustness to unknown external disturbances. In particular, the following contributions can be highlighted.

- The proposed estimator is based on the system's momentum and differs from those already employed in legged robotics. It takes inspiration from estimators already applied in aerial robotics [25]. Such an estimator creates a linear relationship in the Laplace domain. Compared to [25], this paper extends the estimator up to any desired order. The effect of the chosen order on the estimation is also analysed in Section 5.
- The designed framework can deal with disturbances applied both to swing and stance legs, differently to existing approaches mainly coping with disturbances affecting the stance legs only. Indeed, those methods compensating for disturbances acting on the CoM can handle external forces on stance legs, but they cannot compensate for those affecting swing ones and do not prevent foot drifting.
- A method to compensate for external forces acting on swing legs, employing operational space configuration, is presented. The paper aims to demonstrate the consequences of neglecting these disturbances, showing the effect on the robot's balance when planned footholds are not tracked precisely.

The above contributions are validated on an all-ankles configuration quadruped robot within a dynamic simulation environment (see Fig. 1). A comparison with two state of the art approaches bolsters the proposed innovations.

3. Momentum-based estimator of external wrench and unmodelled dynamics

In this section, the model of a legged robot is firstly presented for control design purposes. Afterward, the proposed momentum-based observer is introduced.

3.1. Model formulation

Legged robots are usually modelled as a free-floating base with some legs attached. Let $\mathcal{B}$ be the frame attached to the center of mass (CoM) of the robot (see Fig. 1). The free-floating base is usually modelled through six virtual joints giving six degrees of freedom (DoFs) with respect to a fixed world frame $\mathcal{W}$. Moreover, $n_l \geq 2$ legs are attached to the floating base, giving other nn_l additional DoFs to the structure, where $n > 0$ is the number of joints for each leg.

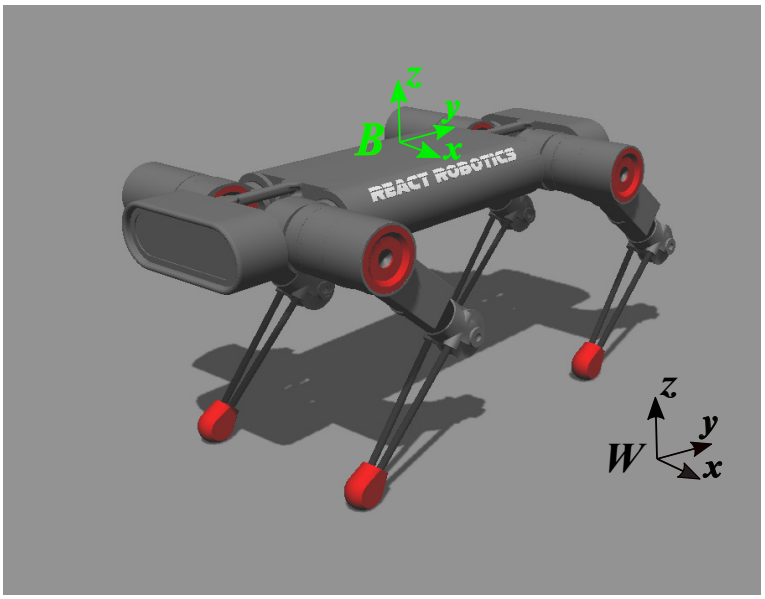

Figure 1: DogBot, the platform used for simulations: reference frames for a floating base robot are shown.

Let $x_{com} = \begin{bmatrix} x_c & y_c & z_c \end{bmatrix}^T \in \mathbb{R}^3$, $\dot{x}_{com} \in \mathbb{R}^3$, and $\ddot{x}_{com} \in \mathbb{R}^3$ be the position, velocity, and acceleration of the frame $\mathcal{B}$'s origin with respect to $\mathcal{W}$, respectively. Besides, let $\omega_{com} \in \mathbb{R}^3$ and $\dot{\omega}_{com} \in \mathbb{R}^3$ be the angular velocity and the angular acceleration of $\mathcal{B}$ with respect to $\mathcal{W}$, respectively. The orientation of $\mathcal{B}$ with respect to $\mathcal{W}$ is expressed by the rotation matrix $R_b \in SO(3)$, from which it can be extracted the set of ZYX Euler angles $\phi \in \mathbb{R}^3$. Finally, indicate with $q \in \mathbb{R}^{nn_l}$ the vector collecting the legs' joints. The dynamic model of a legged robot can be formulated in terms of the global CoM through the transformation introduced in [26]. With this transformation, the inertia matrix assumes the structure $M(q) = \begin{bmatrix} M_{com}(q) & O_{6\times nn_l} \\ O_{nn_l\times 6} & M_q(q) \end{bmatrix} \in \mathbb{R}^{6+nn_l\times 6+nn_l}$. In this way, it is clear the decoupling of the centroidal term $M_{com}(q) \in \mathbb{R}^{6\times 6}$ from the one related to the legs $M_q(q) \in \mathbb{R}^{nn_l\times nn_l}$. To obtain a similar decoupled structure for the vector accounting for Coriolis and centrifugal forces, the assumptions that the main body's angular motion is slow and that the legs' mass is negligible with respect to the robot's total mass are made. As a consequence of these assumptions, the Coriolis and centrifugal terms related to the angular part of the CoM can be neglected [27, 28], obtaining the vector $h(q,\upsilon) = \begin{bmatrix} O_{6\times(6+nn_l)} \\ C_q(q,\upsilon) \end{bmatrix}\upsilon + \begin{bmatrix} mg \\ 0_{nn_l} \end{bmatrix}$, as the sum of Coriolis and centrifugal forces, $C_q(q,\upsilon) \in \mathbb{R}^{nn_l\times(6+nn_l)}$, and gravitational forces where $\upsilon = \begin{bmatrix} \dot{x}_{com}^T & \omega_{com}^T & \dot{q}^T \end{bmatrix}^T \in \mathbb{R}^{6+nn_l}$ is the stacked velocity; vector $m > 0$ is the total mass of the robot, $g = \begin{bmatrix} g_0^T & 0_3^T \end{bmatrix}^T \in \mathbb{R}^6$, and $g_0 \in \mathbb{R}^3$ the gravity vector; $0_\times$ and $O_\times$ the zero vector and matrix of proper dimensions, respectively. The resultant model can be written as

$$M(q)\dot{\upsilon} + h(q,\upsilon) = S^T\tau + J_{st}(q)^T f_{gr} + J(q)^T f_{ext}, \tag{1}$$

with $S = \begin{bmatrix} O_{nn_l\times 6} & I_{nn_l} \end{bmatrix}$ a selection matrix; $\tau \in \mathbb{R}^{nn_l}$ the joint actuation torques; $f_{gr} \in \mathbb{R}^{3n_{st}}$ are the ground reaction forces, with $0 < n_{st} \leq n_l$ the number of stance legs; $J_{st}(q) = \begin{bmatrix} J_{st,com}(q) & J_{st,j}(q) \end{bmatrix} \in \mathbb{R}^{3n_{st}\times 6+nn_l}$ where $J_{st,com}(q) \in \mathbb{R}^{3n_{st}\times 6}$ and $J_{st,j}(q) \in \mathbb{R}^{3n_{st}\times nn_l}$ are those Jacobians whose transpose map the ground reaction forces into the acceleration of the CoM and the legs' joints, respectively; $f_{ext} \in \mathbb{R}^{3n_l}$ is the stacked vector containing the resultant force at the legs' tips accounting for unmodelled dynamics and disturbances at any point of the robot; $J(q) = \begin{bmatrix} J_{com}(q) & J_j(q) \end{bmatrix} \in \mathbb{R}^{3n_l\times 6+nn_l}$ where $J_{com}(q) \in \mathbb{R}^{3n_l\times 6}$ and $J_j(q) \in \mathbb{R}^{3n_l\times nn_l}$ are those Jacobians whose transpose map such external forces into the acceleration of the CoM and the legs' joints, respectively. Further details about the above matrices' expressions can be found in [3, 27, 29].

Notice that, in (1), there is a distinction between the ground reaction forces and the external forces. The former

act only on the stance legs, while the latter accounts for the effects at the legs' tip, including the swing legs, of the disturbances acting at any structure level. As an assumption, the external torques resulting at the legs' tip are negligible. Besides, it can be noticed that the dynamics of the CoM are decoupled from the ones of the legs, so that the CoM's dynamics, also called centroidal dynamics, are included in the first six rows of (1).

3.2. Momentum-based observer

The proposed estimator can reconstruct unknown forces that may arise from several reasons such as unmodelled or inaccurate model parameters, external pushing actions, collisions with obstacles, and so on. These uncertainties are inevitable in the real world. It should be emphasized that, differently from the observers investigated in [1, 2], the one presented in this paper considers the momentum of all the legs, regardless of whether they are stance or swing legs. For this reason, it takes into account the last nn_l rows of (1), recalling that all the disturbances acting on the CoM can be retrieved from forces acting on legs [29].

Suppressing dependencies to compact the notation, the generalized momentum of the legs from (1) can be expressed as

$$\rho = M_q \dot{q}, \tag{2}$$

Taking into account (1), the time derivative of (2) is

$$\dot{\rho} = C_q^T \dot{q} + \tau + J_{st,j}^T f_{gr} + J_j^T f_{ext}, \tag{3}$$

where the property $\dot{M}_q = C_q + C_q^T$ has been taken into consideration in the calculations [30]. Let $\hat{f} \in \mathbb{R}^{3n_l}$ be the estimation of the vector f_{ext}, recalling that it accounts for the resultant effects at the legs' tips of the external forces acting on the structure of the robot. The intention is to reduce the difference between the estimated forces and the real ones. Without loss of generality, define $\hat{F} = J_j^T \hat{f} \in \mathbb{R}^{nn_l}$ and $F_{ext} = J_j^T f_{ext} \in \mathbb{R}^{nn_l}$. This last represents the effect at the joint torques of the resultant force at the legs' tips. In the same way, $\hat{F}$ represents the estimated joint torques corresponding to the resultant at the legs' tips. The estimator is explicitly designed to achieve a linear relationship between the estimated external forces and the real ones in the Laplace domain

$$\hat{F} = G(s) F_{ext}, \tag{4}$$

with $s \in \mathbb{C}$ the complex Laplace variable and $G(s) \in \mathbb{C}^{(nn_l)\times(nn_l)}$ a diagonal matrix of transfer functions. The i-th diagonal element of $G(s)$ is

$$G_i(s) = \frac{k_0}{s^r + c_{r-1}s^{r-1} + \cdots + c_1 s + c_0}, \tag{5}$$

with $i = 1, \ldots, nn_l$, $r > 0$ the desired degree of the estimator, $k_0 > 0$ a gain, and c_j the coefficients of a Hurwitz polynomial, with $j = 0, \ldots, r-1$. Notice that, in principle, the Hurwitz polynomial can change among the single $G_i(s)$. To obtain (5) in the Laplace domain, taking into account (3), the estimator is designed in the time domain as follows

$$\gamma_1(t) = K_1 \left(\rho_j(t) - \int_0^t (\hat{F}(\sigma) + \alpha(\sigma)) \mathrm{d}\sigma \right), \tag{6}$$

$$\gamma_i(t) = K_i \int_0^t (-\hat{F}(\sigma) + \gamma_{i-1}(\sigma)) \mathrm{d}\sigma, \quad i = 2, \ldots, r, \tag{7}$$

where $\hat{F} = \gamma_r$, $K_i \in \mathbb{R}^{(6+nn_l)\times(6+nn_l)}$ are positive definite gain matrices, with $i = 1, \ldots, r$, and

$$\alpha(\sigma) = C_q^T \dot{q} + \tau + J_{st,j}^T f_{gr}, \tag{8}$$

In practical implementation, integrals in (6) and (7) are discretized, while $\hat{F}(\sigma)$ is referred to the estimation obtained at the previous time step.

Notice that, if $r = 1$, only (6) is relevant. Besides, notice that the elements of K_i, with $i = 1, \ldots, r$, are related to the coefficients c_j in (5), with $j = 0, \ldots, r-1$, and it is assumed that $\rho(0) = \gamma_i(0) = 0$, with $i = 1, \cdots, r$, meaning that the estimator's kick off should be prior to the robot control.

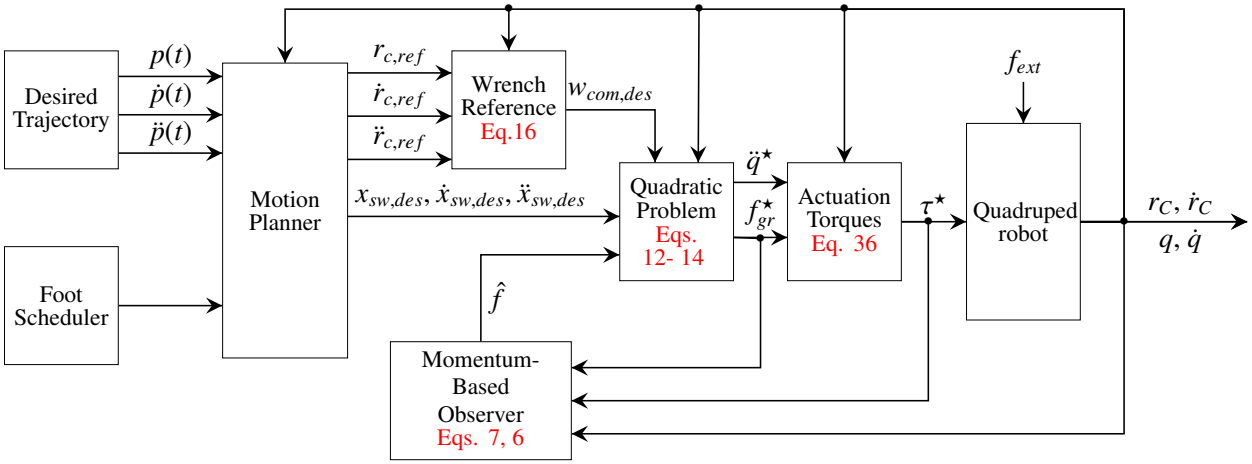

Figure 2: Conceptual block scheme of the devised whole-body controller.

Having in mind (1) and (3), the estimator's dynamics in the time domain can be written in the following compact form

$$\sum_{i=0}^{r} \left(\prod_{j=r}^{i+1} K_j \right) \hat{F}^{(i)} = \prod_{i=1}^{r} K_i F_{ext}, \tag{9}$$

where $\hat{F}^{(i)} = \gamma_{r-i}$ is the i-th time derivative of the $\hat{F}$, with $\hat{F}^{(0)} = \hat{F}$ and $\prod_{j=r}^{r+1} K_j = I_{nn_l}$, with $I_\times$ the identity matrix of proper dimensions. Notice that the estimation of the external forces at the legs' tips can be retrieved through $\hat{f} = J_j^{T^\dagger} \hat{F}$.[1]

The quantities needed to estimate the external force are highlighted in (8). In particular, the proposed estimator needs the knowledge of the joint position, q, and velocity, $\dot{q}$; the legs' input torques, τ; and the ground reaction forces, f_{gr}. The joint position and velocity can be easily obtained from the motors' encoder. The computation of the input torque will be instead described in Section 4. Finally, the ground reaction forces can be obtained by embedded sensors on robot's feet.

4. Controller

The estimator presented above, a motion planner, and an optimization problem shape the designed whole-body controller. The motion planner is thus separated from the control problem. The employed framework is conceptually depicted in Fig. 2. The motion is continuously replanned based on the current robot's state, following a desired trajectory. A foot scheduler is used to switch the stance and swing legs according to the desired gait [13]. Afterward, the motion planner and the quadratic problem are described.

4.1. Motion planning

The motion is continuously replanned so that the ZMP, $x_{zmp} = \begin{bmatrix} x_z & y_z & z_z \end{bmatrix}^T \in \mathbb{R}^3$ expressed in $\mathcal{W}$, is always maintained inside the support polygon [13]. From now on, the position and the orientation of the CoM will be combined into the vector $r_c = \begin{bmatrix} x_{com}^T & \phi^T \end{bmatrix}^T \in \mathbb{R}^6$, with its time derivatives $\dot{r}_c = \begin{bmatrix} \dot{x}_{com}^T & \omega_{com}^T \end{bmatrix}^T \in \mathbb{R}^6$ and $\ddot{r}_c = \begin{bmatrix} \ddot{x}_{com}^T & \dot{\omega}_{com}^T \end{bmatrix}^T \in \mathbb{R}^6$. For each footstep, the motion is split into two phases, replanning the desired trajectory for the CoM at the beginning of each footstep, with a period T_{fs}.

[1] The pseudo-inversion is indicated for the general case, in which ad-hoc solutions can be employed [4, 22, 31, 32]. For the quadruped adopted in this paper, the matrix $J_j \in \mathbb{R}^{12\times12}$ is squared. Singularities are avoided by the gait generator (see Section 5.1)

4.1.1. Stance phase

All the legs are in the stance condition, ensuring an intrinsic balance. Therefore, the reference of the CoM, $r_{c,ref} \in \mathbb{R}^6$ can be computed as a 3-rd order spline that brings it at the center of the support polygon with the desired orientation [14].

4.1.2. Swing phase

At least one leg is swinging. The motion could be quasi-static if only one leg is moving, or highly dynamic if two legs are swinging and the support polygon degenerates into a line. During this phase, both the references for the CoM and the swing feet need to be planned. The reference $x_{sw,des} \in \mathbb{R}^{3(n_l-n_{st})}$ for the swing feet is computed using two splines: the former to lift the foot, the latter to lower it. Considering $T_{sw} > 0$ the duration of the swing phase, each spline lasts $0.5T_{sw}$ [33]. The linear reference of the CoM is instead computed solving an optimization problem, having as variables the coefficients of a third-order spline for each coordinate of the CoM [13]. The problem penalizes the deviation from a regularized path $p(t) \in \mathbb{R}^3$, expressed in $\mathcal{W}$, approximated as a sequence of splines, such that:

- the initial state $p(0)$, $\dot{p}(0)$ and $\ddot{p}(0)$ coincides with $x_{com}(0)$, $\dot{x}_{com}(0)$, and $\ddot{x}_{com}(0)$, respectively;
- the position $p(t_f)$, where $t_f > 0$ is the final time, is set to be at the center of the planned support polygon, while $\dot{p}(t_f)$ and $\ddot{p}(t_f)$ are zero, so that the robot can stop and stand up at the end of the support polygon sequence.

An important constraint during this phase regards the ZMP, that can be written in function of the CoM as following

$$x_z = x_c - \frac{1}{(g_z + \ddot{z}_c)}\left(z_c\ddot{x}_c + \frac{\dot{L}_y}{m}\right), \tag{10}$$

$$y_z = y_c - \frac{1}{(g_z + \ddot{z}_c)}\left(z_c\ddot{y}_c - \frac{\dot{L}_x}{m}\right), \tag{11}$$

with $g_z > 0$ the gravity acceleration and $L = \begin{bmatrix} L_x & L_y & L_z \end{bmatrix}^T \in \mathbb{R}^3$ the angular momentum at the CoM. In the following, it will be assumed $\dot{L} = 0$, since there is no optimization for rotations within the trajectory computation. Considering (10) and (11), the ZMP can be limited inside the support polygon adding a constraint for each of its edges [13]. The angular reference of the CoM is computed as a 3-rd order spline, bringing the robot to the desired orientation.

4.2. Quadratic problem

The optimization problem presented in this paper is wrench-based, and employs the centroidal dynamics only, that is the first six rows of (1). The chosen vector of control variables is $\zeta = \begin{bmatrix} \ddot{r}_c^T & \ddot{q}^T & f_{gr}^T \end{bmatrix}^T \in \mathbb{R}^{6+nn_l+3n_{st}}$. The problem described in the following has the form

$$\underset{\zeta}{\text{minimize}} \quad f(\zeta) \tag{12}$$

$$\text{subject to} \quad A\zeta = b, \tag{13}$$

$$D\zeta \leq c. \tag{14}$$

The detail for each term of the above minimization problem is detailed in the following.

4.2.1. Cost function

The cost function aims at tracking the CoM's reference coming from the motion planner, reducing as much as possible the control effort. To this aim, it is useful to consider the first six equations of (1)

$$M_{com}(q)\dot{v} + mg_0 = w_{com} = J_{st,com}(q)^T f_{gr} + J_{com}(q)^T f_{ext}, \tag{15}$$

where $w_{com} \in \mathbb{R}^6$ is the wrench at the robot's CoM including inertial and gravity terms. Using the references $r_{c,ref}$, $\dot{r}_{c,ref}$, and $\ddot{r}_{c,ref}$ from the motion planner, the desired wrench $w_{com,des} \in \mathbb{R}^6$ can be written as

$$w_{com,des} = K_p(r_{c,ref} - r_c) + K_d(\dot{r}_{c,ref} - \dot{r}_c) + mg + M_{com}(q)\ddot{r}_{c,ref}, \tag{16}$$

with $K_p, K_d \in \mathbb{R}^{6\times6}$ positive definite matrices.

Recalling that $\hat{f}$ is the estimated force vector from the observer presented in Section 3, this can be split into $\hat{f}_{st} \in \mathbb{R}^{3n_{st}}$, the estimated forces regarding the support legs, and $\hat{f}_{sw} \in \mathbb{R}^{3(n_l-n_{st})}$, the estimated forces regarding the swing legs. The cost function minimizing the desired wrench and compensating for the support legs' disturbance is

$$f(\zeta) = \left\| J_{st,com}^T \Sigma\zeta + J_{st,com}^T \hat{f}_{st} - w_{com,des} \right\|_Q + \left\| \zeta \right\|_R, \tag{17}$$

with $\Sigma \in \mathbb{R}^{3n_{st}\times(6+nn_l+3n_{st})}$ a matrix selecting the last $3n_{st}$ elements of ζ, $Q \in \mathbb{R}^{6\times6}$ and $R \in \mathbb{R}^{(6+nn_l+3n_{st})\times(6+nn_l+3n_{st})}$ two symmetric and positive definite matrices that can be used to specify the relative weight between the components of the cost function, and $\|\cdot\|_\times$ the quadratic form with proper matrix.

4.2.2. Equality constraints

Two equality constraints need to be imposed. The first one is the equation of the motion and it constraints the control variables to be consistent with the floating base dynamic in the absence, or perfectly compensated, external disturbances. Such a dynamic regards the first six rows of (1) as follows

$$\begin{bmatrix} M_{com}(q) & 0_{6\times nn_l} & -J_{st,com}(q)^T \end{bmatrix} \zeta = -mg. \tag{18}$$

The second equality constraint guarantees that the contact of the supporting feet is maintained. This holds by imposing their velocity equal to zero as $J_{st,com}(q)\dot{r}_c + J_{st,j}(q)\dot{q} = 0_{3n_{st}}$, whose time derivative is

$$J_{st,com}(q)\ddot{r}_c + \dot{J}_{st,com}(q,\dot{q})\dot{r}_c + J_{st,j}(q)\ddot{q} + \dot{J}_{st,j}(q,\dot{q})\dot{q} = 0_{3n_{st}}. \tag{19}$$

In terms of control variables the above constraint becomes

$$\begin{bmatrix} J_{st,com} & J_{st,j} & O_{3n_{st}\times3n_{st}} \end{bmatrix} \zeta = -\dot{J}_{st,com}(q,\dot{q})\dot{r}_c - \dot{J}_{st,j}(q,\dot{q})\dot{q}. \tag{20}$$

Collecting (18) and (20), the terms in (13) are

$$A = \begin{bmatrix} M_{com}(q) & O_{6\times nn_l} & J_{st,com}(q)^T \\ J_{st,com}(q) & J_{st,j}(q) & O_{3n_{st}\times3n_{st}} \end{bmatrix}, \tag{21}$$

and

$$b = -\begin{bmatrix} mg \\ \dot{J}_{st,com}(q,\dot{q})\dot{r}_c + \dot{J}_{st,j}(q,\dot{q})\dot{q} \end{bmatrix}. \tag{22}$$

4.2.3. Inequality constraints

Ground reaction forces need to be constrained inside a friction cone to avoid slipping. For control design purposes, the friction cone is approximated as a pyramid to obtain linear constraints in the optimization problem. Considering the i-th ground reaction force $f_{gr,i} \in \mathbb{R}^3$, with $i = 1,\dots,n_{st}$, and indicating with $\bar{n}_i \in \mathbb{R}^3$ the i-th normal vector, $\bar{l}_{1,i}, \bar{l}_{2,i} \in \mathbb{R}^3$ two tangential vectors related to the i-th contact with the ground, and $\mu > 0$ the friction coefficient, the contact constraints can be written as follows [12]

$$\begin{aligned} (\bar{l}_{1,i} - \mu\bar{n}_i)^T f_{gr,i} &\le 0, \\ -(\bar{l}_{1,i} + \mu\bar{n}_i)^T f_{gr,i} &\le 0, \\ (\bar{l}_{2,i} - \mu\bar{n}_i)^T f_{gr,i} &\le 0, \\ -(\bar{l}_{2,i} + \mu\bar{n}_i)^T f_{gr,i} &\le 0. \end{aligned} \tag{23}$$

Moreover, for mechanical and safety reasons, joint torques need always to be limited. Being $\tau_{min}, \tau_{max} \in \mathbb{R}^{nn_l}$ the minimum and maximum reachable torques, respectively, considering the part of (1) regarding robot's legs, the constraints about limited torques can be expressed as follows

$$\tau_{min} - C_q(q,v)\dot{q} \le \begin{bmatrix} M_q(q) & -J_{st,j}(q)^T \end{bmatrix} \begin{bmatrix} \ddot{q} \\ f_{gr} \end{bmatrix} \le \tau_{max} - C_q(q,v)\dot{q}. \tag{24}$$

The last addressed constraint allows the robot to follow the trajectory planned for the swing feet. This constraint exploits the estimation of external forces from the observer acting on swing legs. These disturbances can heavily affect the respective foot's motion, so it is necessary to compensate for them. For this purpose, operational space formulation for swing feet is now employed. Having (1) in mind, the contact constraints $J_{st}^T f_{gr}$ can be eliminated using an orthogonal projection operator $P \in \mathbb{R}^{6+nn_l \times 6+nn_l}$, such that $PJ_{st}^T = 0$, $P = P^2$, and $P = P^T$ [8, 34]. Although different valid choice can be used for P [35, 36], the matrix P in this paper has been chosen as in [34], that is $P = I_{6+nn_l} - J_{st}^{\dagger} J_{st}$. Pre-multiplying both sides of (1) by P yields

$$P\left(M\dot{\upsilon} + h\right) = PS^T\tau + PJ_{sw}^T f_{sw,ext}. \tag{25}$$

It is worth noticing that, since $PJ_{st}^T = 0$, the only remaining term related to external forces is $J_{sw}^T f_{sw,ext}$, which regards the swing legs. Following [34], equation (25) can be transformed into

$$M_c\dot{\upsilon} + Ph - C\upsilon = PS^T\tau + PJ_{sw}^T f_{sw,ext}, \tag{26}$$

where $M_c = PM + I_{6+nn_l} - P$ and $C = -J_{st}^{\dagger}\dot{J}_{st}$. As discussed in [34], M_c is always invertible, provided that M is invertible. Let $x_{sw} \in \mathbb{R}^{3(n_l-n_{st})}$ be the the position of the swing feet. The following relations hold

$$\dot{x}_{sw} = J_{sw}\upsilon, \tag{27}$$

$$\ddot{x}_{sw} = J_{sw}\dot{\upsilon} + \dot{J}_{sw}\upsilon. \tag{28}$$

Pre-multiplying both sides of (26) by $J_{sw}M_c^{-1}$ and substituting (28) into (26), the following operational space configuration for the swing legs can be recovered

$$\ddot{x}_{sw} - \dot{J}_{sw}\upsilon + J_{sw}M_c^{-1}\left(Ph - C\upsilon\right) = J_{sw}M_c^{-1}PS^T\tau + J_{sw}M_c^{-1}PJ_{sw}^T f_{sw,ext}. \tag{29}$$

The command acceleration for the swing feet $\ddot{x}_{sw,c} \in \mathbb{R}^{3(n_l-n_{st})}$ can be chosen as

$$\ddot{x}_{sw,c} = \ddot{x}_{sw,des} + K_{d,sw}(\dot{x}_{sw,des} - \dot{x}_{sw}) + K_{p,sw}(x_{sw,des} - x_{sw}), \tag{30}$$

with $K_{p,sw}, K_{d,sw} \in \mathbb{R}^{3(n_l-n_{st})\times 3(n_l-n_{st})}$ positive definite matrices. To compensate for disturbances, the term related to external forces on swing legs in (29) must be taken into account. Therefore, the command acceleration needs to become

$$\ddot{x}_{sw,cmd} = \ddot{x}_{sw,c} - J_{sw}M_c^{-1}PJ_{sw}^T\hat{f}_{sw}. \tag{31}$$

To follow the trajectory, the following equality constraint should be imposed, replacing (31) into (28)

$$\ddot{x}_{sw,cmd} = J_{sw,com}(q)\ddot{r}_c + \dot{J}_{sw,com}(q,\dot{q})\dot{r}_c + J_{sw,j}(q)\ddot{q} + \dot{J}_{sw,j}(q,\dot{q})\dot{q}. \tag{32}$$

The constraint is softened by adding slack variables $\gamma \in \mathbb{R}^{3(n_l-n_{st})}$ within the optimization problem. The addressed inequality constraint is thus chosen as [3]

$$\ddot{x}_{sw,cmd} - \gamma \leq J_{sw,com}(q)\ddot{r}_c + \dot{J}_{sw,com}(q,\dot{q})\dot{r}_c + J_{sw,j}(q)\ddot{q} + \dot{J}_{sw,j}(q,\dot{q})\dot{q} \leq \ddot{x}_{sw,cmd} + \gamma. \tag{33}$$

Therefore, collecting (23), (24), and (33), the terms in (14) are

$$D = \begin{bmatrix} O_{4n_{st}\times 6} & O_{4n_{st}\times nn_l} & D_{fr} \\ O_{nn_l\times 6} & M_q(q) & -J_{st,j}^T \\ O_{nn_l\times 6} & -M_q(q) & J_{st,j}^T \\ J_{sw,com} & J_{sw,j} & O_{3(n_l-n_{st})\times 3n_{st}} \\ -J_{sw,com} & -J_{sw,j} & O_{3(n_l-n_{st})\times 3n_{st}} \end{bmatrix}, \tag{34}$$

$$c = \begin{bmatrix} 0_{4n_{st}} \\ \tau_{max} - C_q(q,\upsilon)\dot{q} \\ -(\tau_{min} - C_q(q,\upsilon)\dot{q}) \\ \ddot{x}_{sw,cmd} + \gamma - \dot{J}_{sw,com}(q,\dot{q})\dot{r}_c - \dot{J}_{sw,j}(q,\dot{q})\dot{q} \\ -\ddot{x}_{sw,cmd} + \gamma + \dot{J}_{sw,com}(q,\dot{q})\dot{r}_c + \dot{J}_{sw,j}(q,\dot{q})\dot{q} \end{bmatrix}, \tag{35}$$

where $D_{fr} \in \mathbb{R}^{4n_{st}\times 3n_{st}}$ is a diagonal matrix containing the friction cone constraints expressed in (23) for each stance leg [3].

4.2.4. Control torques

The result of the optimization problem is the desired vector $\zeta^* = \begin{bmatrix} \ddot{r}_c^{\star T} & \ddot{q}^{\star T} & f_{gr}^{\star T} \end{bmatrix}^T$. The control torques can be computed using the second part of (1), considering that all the external forces have been compensated for inside the quadratic problem

$$\tau^* = M_q(q)\ddot{q}^\star + C_q(q, v)\dot{q} - J_{st,j}(q)^T f_{gr}^\star. \tag{36}$$

5. Case studies

In the following, the setup used to test the case studies is presented. An analysis regarding the estimator's order is performed and five case studies are analysed. It will be highlighted how the momentum-based observer presented in this work and integrated into the described whole-body controller allows for achieving better results than two solutions available within the state of the art. The multimedia attachment shows the results of the addressed case studies.

5.1. Setup

Simulations have been carried out through the ROS middleware, in combination with the dynamic simulator *Gazebo*. This choice has been made since Gazebo uses a high-performance physics engine to make the movement and external conditions as realistic as possible. The quadruped used for simulations in Gazebo is DogBot from React Robotics, an open-source platform. The structure of the robot is shown in Fig. 1. It presents three actuated revolute joints for each leg: the first one connects the body with the leg, and its axis is parallel to the longitudinal axis of the body, realizing all the lateral movement; the second and the third ones allow the lift-off of the foot from the ground and coincide with the hip and the knee, respectively, and their axis are both normal to the plane of the leg. Then, for this robot, $n_l = 4$ and $n = 3$. DogBot's configuration has all the legs pointing backward so that the push-off impulse is facilitated, while fast motions are easy to realize. It weighs 21 kg, the mass is mainly concentrated in the body, which has a weight of 12 , while each leg is 2 kg. Both the upper and the lower segments of each leg have a length of around 0.3 m.

All the simulations were performed on a standard personal computer. The references for the CoM and the swing feet were generated using *Towr* [37], a C++ library for trajectory optimization for legged robots. A fixed planned step's height for the swing feet has been set to 0.05 m, and the maximum step length is chosen to avoid a complete stretching or retraction of the legs: at the planning level, this avoids singularities in J_j. Besides, these references were replanned at the beginning of each footstep, with a period $T_{fs} = 0.26$ s. The quadratic problem was solved using the C++ library *ALGLIB*. All the simulations have been tested with crawl and trot gaits. The results here reported regards the trot gait only. Since this gait is dynamic, it can be considered a significant testbed to check the proposed whole-body control's performance.

The gains for the desired wrench in (16) have been experimentally tuned to $K_p = \text{diag}(250, 250, 250, 250, 250, 250)$ and $K_d = \text{diag}(50, 50, 50, 50, 50, 50)$. The gains for the command acceleration for swing feet in (30) have been experimentally tuned to $K_{d,sw} = 100 I_{3n_l - n_{st}}$ and $K_{p,sw} = 25 I_{3n_l - n_{st}}$. The gains for the optimization have been set as $Q = \text{diag}(100, 100, 100, 100, 100, 100)$, $R = I_{6+nn_l+3n_{st}}$, while $\mu = 1.0$, $\tau_{min} = -60$ Nm, and $\tau_{max} = 60$ Nm. The stance phase has been chosen to last 0.15 s, while the swing phase lasts 0.115 s. Numerical integration for dynamics is set in Gazebo as $\delta\, t = 0.001$ s.The torque control loop, the state estimation and the momentum-based observation have a frequency of 1 kHz, while the optimization problem runs at a frequency of 400 Hz. The various operations of the control scheme are applied sequentially.

In order to test the whole-body control design, six case studies have been considered. A sinusoidal disturbance with an amplitude of 20 N has been applied on the front left knee within the first case study. In the second case study, the same sinusoidal disturbance has been applied to carry out a comparison against two state-of-the-art solutions. In the third case study, instead, a disturbance of 80 N has been applied for a small portion of time, 0.2 s, on the front right knee during his swing phase, simulating a sudden impact. In the fourth case study, a random disturbance is injected every two seconds on a randomly chosen leg. The force is applied at different points of the limb to show the effectiveness of the approach. This situation is repeated in the fifth case study, where this random disturbance is combined with parametric uncertainties in the model known by the controller. Finally, the robot is tested on an irregular terrain. In all these cases, the norm is Euclidean.

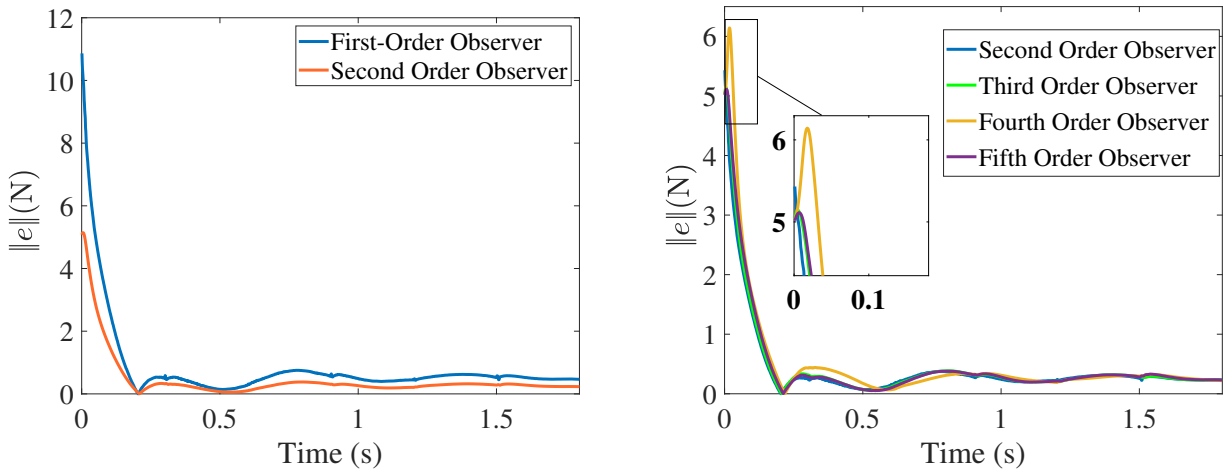

Figure 3: Analysis on the order of the estimator. (a) Estimation's error for first (blue) and second (orange) order. (b) Estimation's error for second (blue), third (green), fourth (yellow) and fifth (violet) order.

Although the estimated vector accounts for the effects at the legs' tips of external forces acting at any point of the robot (information that is unknown by the controller), the plots presented in the following show the estimated force vector reported back to the application point of the disturbance. This is obtained after offline post-processing of the results.

5.2. Analysis on the order of the estimator

A series of simulations have been done to choose the estimator's order, considering a constant external force. The estimation's error for different orders is reported in Fig. 3. In Fig. 3a, a comparison has been made between first-order and second-order estimators. It can be noticed that the former presents a higher overshoot of the error. Results for the next orders are shown in Fig. 3b. From the third-order, it is not possible to appreciate any significant improvement. Anyway, the overshoot of the error is higher for the fourth and second order. For this reason, the best choices are the third and fifth orders. In this paper, as a result of the analysis carried out, the degree r is set to 3, while coefficients K_1, K_2 and K_3 have been chosen as $17.5I_{12}$, $6.28I_{12}$ and $2.25I_{12}$, respectively, in a trade-off between desired results and the computational time leading to delays.

5.3. Case Study 1

The first case study has been carried out by considering a sinusoidal disturbance along the x-axis, with an amplitude of 20 N and a period $T = 2\pi$ s, on the front left knee during all the simulation. This choice is made to see the effect of time-varying disturbances on a leg during both the stance and the swing phase. In this case study, the robot is guided to follow a trajectory of 5.5 m composed of alternating sequences of rectilinear and curvilinear motions. The forward velocity is 0.12 m/s and, during curvilinear motions, the angular velocity is 0.05 rad/s.

A simulation of this case study without counterbalancing for disturbances on the swing legs is performed and presented in the multimedia attachment to stress the importance of having such compensation. It could be observed that, although the robot can retain the balance for a while, the drift of the perturbed leg's foot is evident. It brings the robot to fall after 11.3 s. Fig. 4 shows in detail this situation with a series of pictures of salient instants of the movement.

Using the proposed framework, this situation can be avoided. The norm of CoM error for a portion of the path is shown in Fig. 5. It can be noticed that, although the error is at most 0.01 m, some peaks can be noticed: these are produced during the swing phase regarding the front leg subject to the external disturbance. In general, the CoM error components have sinusoidal trend. This is given by the continuous change of support legs, so the motion of the

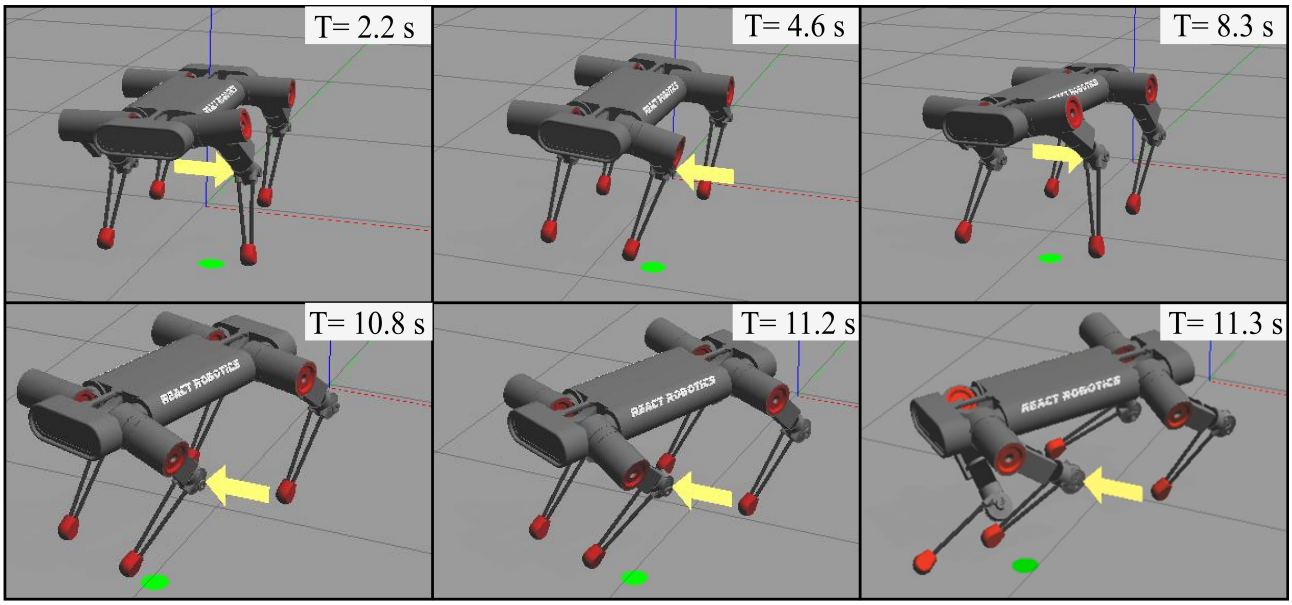

(a)

Figure 4: Case Study 1. In this simulation, external forces on swing legs are not compensated. These pictures show instants when the disturbance is around its peaks. The yellow arrow indicates the application point and direction of the force. The green circle represents the planned foothold, the drift of the foot is evident. At 11.3 s, the robot loses its balance.

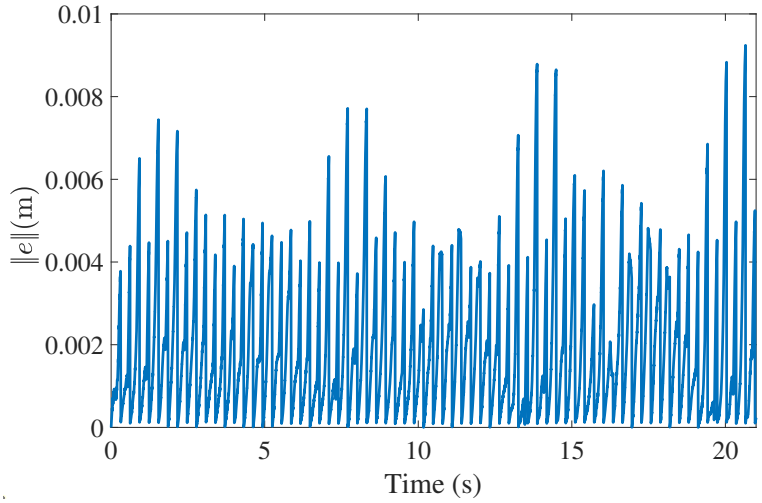

Figure 5: Case Study 1. Error norm of the robot's CoM using the proposed whole-body controller.

CoM is replanned to reach the center of the current support polygon. During the swing phase, the support line has been enlarged to a rectangle to soften the constraint about the ZMP. The disturbance reconstructed by the observer is depicted in Fig. 6. Small uncertainties can be noticed, probably given by some parametric inaccuracies in the model.

Fig. 7 shows the norm of the error between the ground reaction forces computed by the QP (12)-(14) and the ones measured by some sensors put under the feet within the Gazebo environment. The time history is referred to the front left leg so as to prove the framework's effectiveness in tracking the ground reaction forces. The average of such error remains under 5 N, which is an improvement with respect to existing works [2].

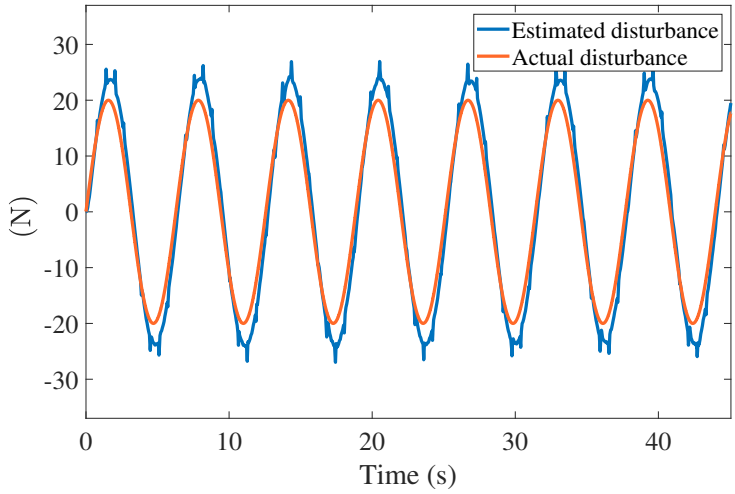

Figure 6: Case Study 1. Estimation of the disturbance through the proposed momentum-based observer. In blue the estimated force, in orange the actual force.

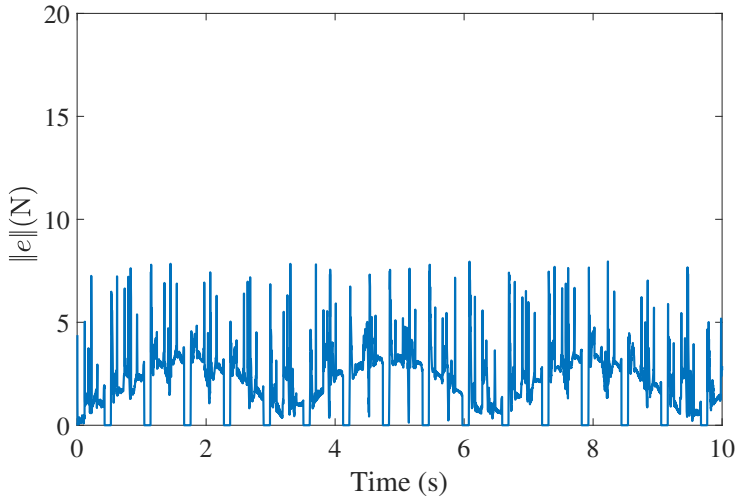

Figure 7: Case Study 1. Error norm of the ground reaction forces for front left leg, using the proposed whole-body controller.

5.4. Case Study 2

A comparison with state-of-the-art observers is now accomplished to validate the envisaged whole-body controller's performance further. Both the trajectory and the external disturbance are the ones considered in case study 1. The observers chosen for comparison are picked up from [2] and [24]. The former is a first-order momentum observer that considers only the external wrench of the CoM and can deal with disturbance applied to the stance legs only. This is reasonable in those cases where the only source of errors comes from the unknown terrain. This observer employs the first six rows from (1). The latter observer is a nonlinear disturbance observer taking into account the four legs' dynamics, but it is not based on the system's momentum. To the best of authors' capabilities, the gains for the first observer were chosen as $G_{lin} = 25I_3$ and $G_{ang} = 10I_3$ [2], while for the second observer the the gain matrix was set as $X = 10I_{12}$. The gains of the optimization problem remain unchanged.

The norm of the CoM errors of the three considered observers is compared in Fig. 8. It can be noticed that observer from [2] and the one from [24] have similar CoM error norm. Nevertheless, the former is not able to follow

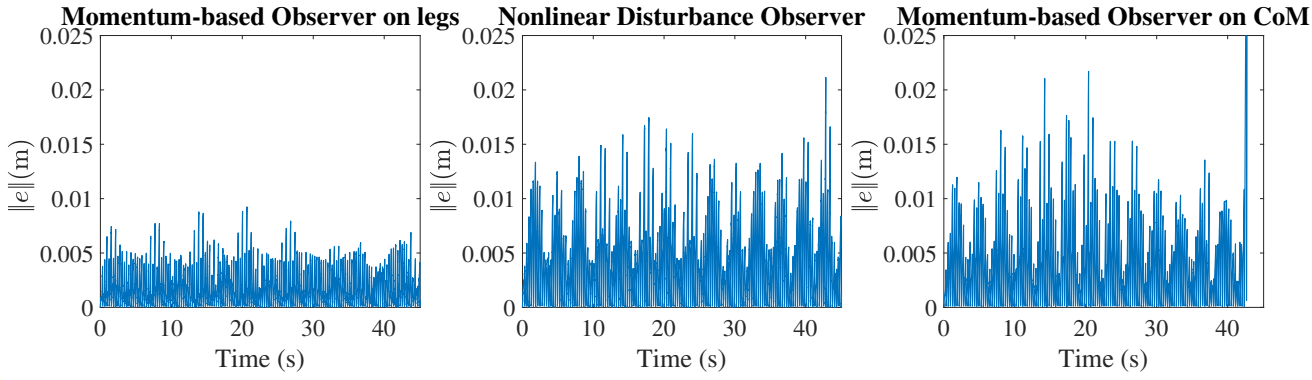

Figure 8: Case Study 2. Comparison between several control techniques. The plot show the error norm of the robot's CoM for each of the considered observer. From left to right: the results obtained with the proposed controller; the results obtained using [2]; the results obtained through [24].

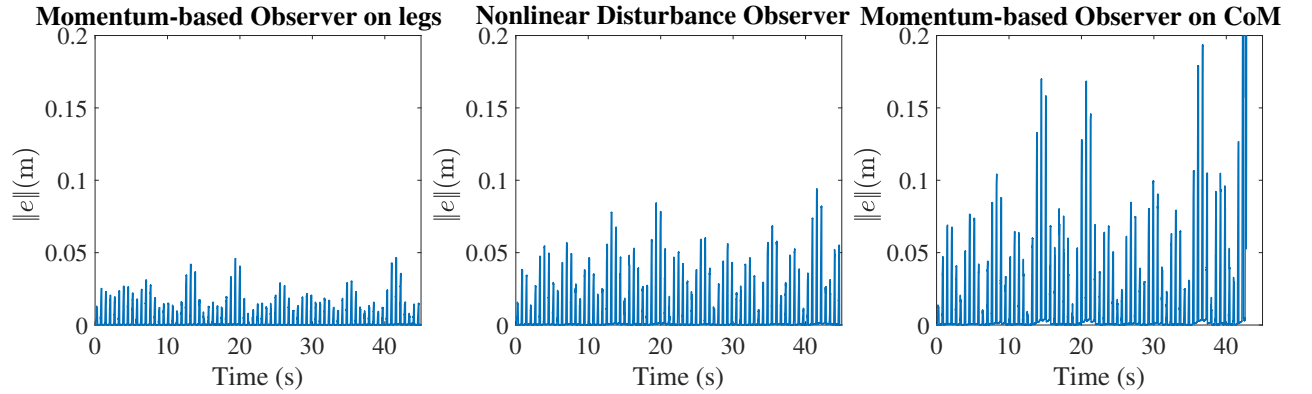

Figure 9: Case Study 2. Comparison between several control techniques. The plot shows the error norm of the front left foot position for each of the considered observer. From left to right: the results obtained with the proposed controller; the results obtained using [2]; the results obtained through [24].

the full trajectory. Indeed, as can be seen in the video at 42.6 s, the robot loses its balance. An explanation of this imbalance can be found in Fig. 9, where the error norm of the front left foot position is represented. It can be seen that the highest error norm of the foot position is obtained using the observer proposed in [2]. As it was already said, this is the only observer, here tested, that considers only the external wrench of the CoM. Using this observer, the disturbance on the leg causes a significant drift of the foot during the swing phase, which, although the CoM error remains small, brings to the loss of balance. It is highlighted once again the importance of considering leg dynamics and compensating for external forces on all the legs. Given the authors' ability to implement and tune the addressed state-of-the-art observers, the proposed observer seems to outperform the others thanks to explicitly addressing the errors on the swing legs. This is evident since the error norm on the robot's CoM is less than 0.01 m and the error norm of the foot position subject to the disturbance is always less than 0.05 m.

5.5. Case Study 3

Within the third case study, a brief but severe disturbance is applied along the x-axis on the front right knee during its swing phase. The planned trajectory is a rectilinear path and the forward velocity is 0.12 m/s. The disturbance has a magnitude of 80 N, it lasts for 0.2 s, and it is injected at 2.8 s from the planned trajectory's start. The instant of the injection has been chosen so that it goes to apply on the leg during its swing phase, demonstrating that the control framework can handle unexpected impulsive disturbances.

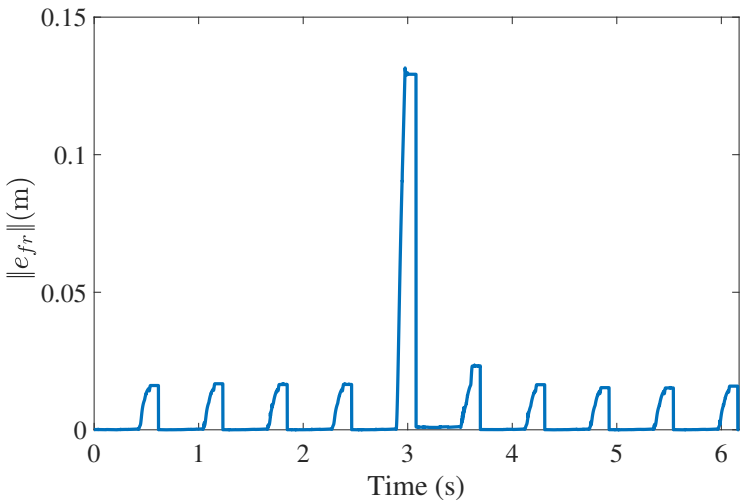

Figure 10: Case Study 3: Error norm of the front right foot position using the proposed whole-body controller.

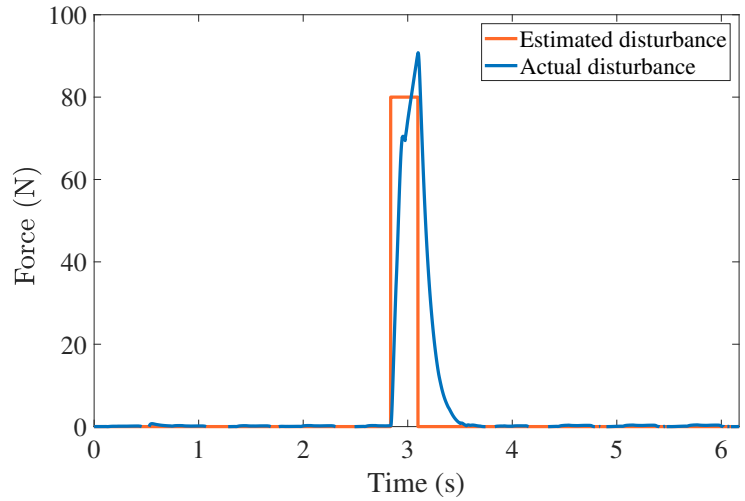

Figure 11: Case Study 3: Estimation of the disturbance through the proposed momentum-based observer. In blue the estimated force, in orange the actual force.

This time, only the results regarding the whole-body control here introduced will be shown, since the two state-of-art observers considered above cannot deal with such a significant disturbance (see the multimedia attachment), which resembles an impulsive behavior, like a pushing action. It can be seen that such a disturbance causes a considerable drift of the front right foot while it is swinging, unbalancing the robot.

The controller here presented can instead cope with such a disturbance by minimizing the leg's drift and recovering the given trajectory in the next footsteps. This can be appreciated in Fig. 10, where the foot position's error is shown. The highest peak coincides with the application of the disturbance. Fig. 11 shows the estimation of the external force, while in Fig. 12 the CoM's error norm can be observed. In this case, there are two peaks: the first one is caused by the external force, while the second coincides with the recovery footstep, a phase in which the support polygon is not optimal given the former drift of the foot subject to the disturbance. However, the CoM's error is still less than 0.01 m, guaranteeing the recovery of the balance after the impact.

This third case study demonstrates that the designed architecture can effectively estimate a large disturbance, also

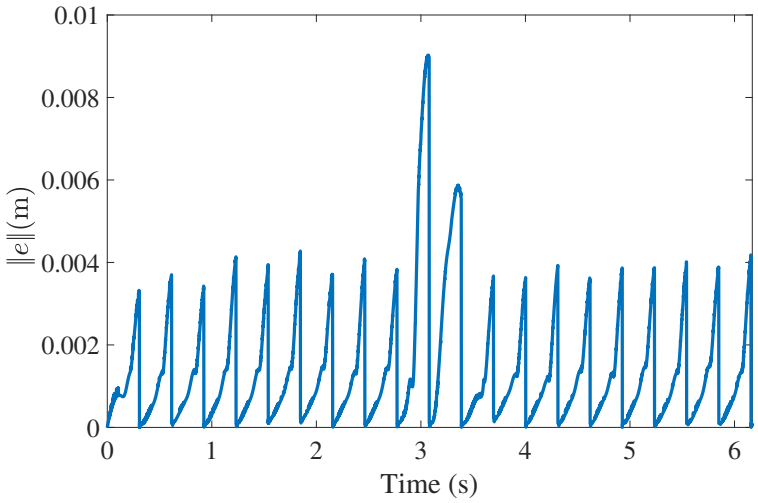

Figure 12: Case Study 3: Error norm of the robot's CoM using the proposed whole-body controller.

if it happens on a leg during its swing phase. In this way, the legged robot can work in various scenarios: for instance, in severe atmosphere conditions or during collisions with the environment during the swinging. The disturbance's magnitude has been chosen so large on purpose to bolster the performance of the envisaged observer that can cope with a broader range of disturbances than other state-of-art observers, which can handle only small external forces acting on swing legs.

5.6. Case Study 4

The fourth case study has been carried out considering a random disturbance. Every two seconds, the force's magnitude changes randomly between 10 N and 35 N. Moreover, both the leg subject to the perturbation and the height of the application point change too. The direction of the disturbance forces is shown in the multimedia attachment.

In this case study, the robot is guided to follow a trajectory of 3.7 m composed of alternating sequences of rectilinear and curvilinear motions. The forward velocity is 0.12 m/s and, during curvilinear motions, the angular velocity is 0.05 rad/s.

This case has been tested only using the whole-body controller proposed. This case study aims to demonstrate the validity of the proposed method for a wide range of disturbances. The approach results robust against a random perturbation and also against an unexpected variation of the application point. The location of the external force is chosen along all the length of the legs. It could be from the top (so it can be considered a disturbance on the torso) to the bottom (at the foot). In this way, the observer helps with general disturbance rejection where external forces can be applied anywhere on the robot.

In Fig. 15a the plot about the error norm of the CoM is reported. It can be observed that the peaks of error are always around 0.01 m. Nevertheless, in previous cases has been highlighted the importance of foot position error, that can cause a loss of balance even if the CoM error is small. For this reason, in Fig. 13, the disturbances for each leg are represented on the right. On the left, the norm errors of the respective foot can be observed, so that it can be noticed that the highest peaks correspond to the application of the external force on the leg. In particular, it can be observed that the error is always under 0.035 m except for cases when the start of disturbance application coincides with the beginning of the swing phase. This situation verifies for the front left foot at 10 s and the rear right foot at 26 s. In these instants, the unexpected and instantaneous disturbance is applied to the leg while its foot lifts off the ground. Since this external force is not compensated, the foot is subject to an initial drift higher than usual. Anyway, the observer demonstrates to estimate the disturbance in a short time so that the balance can be retained.

Until now, all the cases have been simulated in an ideal situation. In a real situation, some sensor noise could influence the estimation of the observer, adding uncertainty. For this reason, this case has also been tested in a non-ideal condition, adding a white Gaussian noise on both the joint torque and the ground reaction forces measurements with

a standard deviation of 10% of the measured signal. This situation has been tested to analyze further the robustness of the controller. In Fig. 14 the plot about the disturbance estimation for each leg is reported alongside the norm error of the respective foot. In this case, it can be noticed that the presence of noise inevitably leads to a noisy estimation. However, the controller can still guarantee an optimal tracking of the feet position. Its error is below 0.06 m, except for cases when the disturbance application coincides with the swing phase's beginning. Also, good tracking of the CoM is performed, as can be observed in Fig. 15b, where the peaks of error are always less than 0.014 m.

5.7. Case Study 5

The fifth case study considers the same random disturbance of the fouth case study. Now, to add a parametric uncertainty, the total mass known by the controller is changed by 30%.

While the goal of case study 4 was to demonstrate the validity of the approach for external forces applied at different points, this case study aims to extend the range of disturbances considering parametric uncertainties in the model.

As in the previous case, the disturbances for each leg and the respective foot's norm errors are represented in Fig. 16. It is worth noticing that, this time, the estimated force has an offset due to the parametric error, which is seen as a disturbance even when there is no physical force applied to the robot. This can be appreciated in Fig. 16g: no perturbation is acting on the rear right leg, but the estimation is never equal to zero. The norm error of the feet position is always less than 0.035 m, guaranteeing a precise tracking of the support polygon desired. As highlighted in the previous case, some peaks of the error happen when the beginning of the swing phase and the disturbance's application coincide. In Fig. 17 the plot about the error norm of the CoM is reported. It can be observed that the peaks of error are now higher, but always less than 0.015 m. This small increment of the error can be considered the result of the parametric uncertainty, which can still be handled.

5.8. Case Study 6

The sixth case study focuses on the capability of the whole-body controller to work on irregular terrain. For this purpose, some blocks with different heights have been added to the environment to reproduce the terrain's irregularities, as it is shown in Fig. 18. Moreover, all the blocks have different friction coefficients to simulate various kinds of soils. With reference to the figure, the heights of the blocks are 0.015 m for blue blocks, 0.04 m for green blocks, and 0.02 m for red blocks. Instead, the friction coefficients are 0.4 for blue blocks, 0.6 for green blocks, 0.8 for red blocks, and 1 for the ground. These friction coefficients have been chosen after different simulations, which demonstrated the approach could not guarantee good performance for coefficients lower than 0.4. For smaller coefficients, it is possible to retain the balance, but there is a foot slipping after the impact phase. The friction coefficient inside the whole-body controller has been chosen, in a conservative way, as 0.4. This is crucial to improve robustness so that the controller can step over different soils without slipping, maintaining the ground reaction forces inside the friction cone. In this case, the path is rectilinear and the forward velocity is 0.12 m/s.

The results of this case study demonstrate the capability of the proposed approach to reject disturbances given by an irregular terrain. In particular, these external forces are given by the anticipated touchdown caused by different heights of the soil. Indeed, the reference foothold is planned for a flat ground, and the unexpected difference in the height causes an asymmetric gait, unbalancing the robot. This concept can be appreciated in Fig. 19, where the foot's norm error for each leg is shown. It can be noticed that, differently from other cases, the are some intervals where the foot's norm error never goes to zero despite the re-planning (e.g., from instant $t_1 = 10$ s to $t_2 = 20$ s in Fig. 19a). Comparing the figure with the video shows that these intervals coincide with the stepping of the respective foot on one of the blocks. During these phases, the block's height constitutes a continuous disturbance since the reference foothold is planned for a flat ground. Observing the figure, it could be noticed that the height of different blocks can be retrieved from the position error. It should also be noticed that the heights of the blocks have been chosen considering the planned step's height. In the case of a high block, there would be the need for a strategy for recognition of the height and a consequent adjustment of the gait. However, this is out of the scope of this paper. In Fig. 20, it can be observed that the controller, despite the irregularities, guarantees a good tracking of the CoM position, with an error always less than 0.01 m. In the multimedia attachment, some instants are highlighted when a foot impact the edge of a block or slide down between two blocks. Nevertheless, in all these cases, the balance is retained, demonstrating the robustness of the controller.

6. Conclusion and future work

In this work, a momentum-based observer was proposed for a quadruped robot. Such an observer is integrated into a whole-body controller, which compensates for external forces acting on both stance and swing legs. The operational space configuration for swing feet was employed to compensate for disturbances affecting swing legs. The observer was tested against two state-of-art observers, demonstrating satisfactory performance in reacting to time-varying external forces. Indeed, it appears to reduce the error to the planned robot's CoM and improve the stability, even if the swing leg is affected by large and impulsive external unpredicted forces. The proposed approach was also tested with random forces, demonstrating its robustness against both an unexpected variation of the application point and parametric uncertainties. The controller resulted in being robust against noisy measurement and on irregular terrain.

The controller allows the locomotion of a legged robot inside an unstructured environment where a collision could happen. Indeed, if a swing leg impacts an object, it is possible to have a wide drift of the foot. It causes a reduction of the support polygon, unbalancing the robot. The controller presented compensate directly for those disturbances acting on the moving legs, minimizing the drift. Beyond the presence of obstacles, the controller guarantees good performance when irregularities in the terrain cause the disturbance. Nevertheless, the approach cannot handle obstacles higher than the planned step. In this case, there would be the need to recognize the height and adjust the gait to overcome the obstacle. Although this approach can prevent the sliding of feet for a wide range of surfaces, it can not avoid sliding for grounds with a friction coefficient of less than 0.4. On these surfaces, a sliding after the impact phase happens, leading the robot to fall.

In the future, this observer might be used within legged manipulation scenarios, where the legged robot is equipped with a manipulator's arm. In this case, the observer would allow decoupling the manipulation task from locomotion.

References

[1] J. Englsberger, G. Mesesan, C. Ott, Smooth trajectory generation and push-recovery based on divergent component of motion, in: 2017 IEEE/RSJ International Conference on Intelligent Robots and Systems, 2017, pp. 4560–4567.

[2] M. Focchi, R. Orsolino, M. Camurri, V. Barasuol, C. Mastalli, D. G. Caldwell, C. Semini, Heuristic planning for rough terrain locomotion in presence of external disturbances and variable perception quality, in: Advances in Robotics Research: From Lab to Market, 2020, pp. 165–209.

[3] S. Fahmi, C. Mastalli, M. Focchi, C. Semini, Passive whole-body control for quadruped robots: Experimental validation over challenging terrain, IEEE Robotics and Automation Letters 4 (3) (2019) 2553–2560.

[4] N. Dini, V. J. Majd, F. Edrisi, M. Attar, Estimation of external forces acting on the legs of a quadruped robot using two nonlinear disturbance observers, in: 2016 4th International Conference on Robotics and Mechatronics, 2016, pp. 72–77.

[5] N. Dini, V. J. Majd, An MPC-based two-dimensional push recovery of a quadruped robot in trotting gait using its reduced virtual model, Mechanism and Machine Theory 146 (2020).

[6] A. W. Winkler, F. Farshidian, M. Neunert, D. Pardo, J. Buchli, Online walking motion and foothold optimization for quadruped locomotion, in: 2017 IEEE International Conference on Robotics and Automation, 2017, pp. 5308–5313.

[7] O. E. Ramos, N. Mansard, P. Soueres, Whole-body motion integrating the capture point in the operational space inverse dynamics control, in: 2014 IEEE International Conference on Humanoid Robots, 2014, pp. 707–712.

[8] M. Hutter, H. Sommer, C. Gehring, M. Hoepflinger, M. Bloesch, R. Siegwart, Quadrupedal locomotion using hierarchical operational space control, The International Journal of Robotics Research 33 (8) (2014) 1047–1062.

[9] G. Xin, H.-C. Lin, J. Smith, O. Cebe, M. Mistry, A model-based hierarchical controller for legged systems subject to external disturbances, in: 2018 IEEE International Conference on Robotics and Automation, 2018, pp. 4375–4382.

[10] G. Xin, W. Wolfslag, H.-C. Lin, C. Tiseo, M. Mistry, An optimization-based locomotion controller for quadruped robots leveraging Cartesian impedance control, Frontiers in Robotics and AI 7 (2020) 1–12.

[11] W. Du, M. Fnadi, F. Benamar, Rolling based locomotion on rough terrain for a wheeled quadruped using centroidal dynamics, Mechanism and Machine Theory 153 (2020).

[12] C. D. Bellicoso, C. Gehring, J. Hwangbo, P. Fankhauser, M. Hutter, Perception-less terrain adaptation through whole body control and hierarchical optimization, in: 2016 IEEE-RAS 16th International Conference on Humanoid Robots, 2016, pp. 558–564.

[13] C. D. Bellicoso, F. Jenelten, P. Fankhauser, C. Gehring, J. Hwangbo, M. Hutter, Dynamic locomotion and whole-body control for quadrupedal robots, in: 2017 IEEE/RSJ International Conference on Intelligent Robots and Systems, 2017, pp. 3359–3365.

[14] C. D. Bellicoso, F. Jenelten, C. Gehring, M. Hutter, Dynamic locomotion through online nonlinear motion optimization for quadrupedal robots, IEEE Robotics and Automation Letters 3 (3) (2018) 2261–2268.

[15] G. Bledt, P. M. Wensing, S. Kim, Policy-regularized model predictive control to stabilize diverse quadrupedal gaits for the MIT Cheetah, in: 2017 IEEE/RSJ International Conference on Intelligent Robots and Systems, 2017, pp. 4102–4109.

[16] J. Koenemann, A. Del Prete, Y. Tassa, E. Todorov, O. Stasse, M. Bennewitz, N. Mansard, Whole-body model-predictive control applied to the hrp-2 humanoid, in: 2015 IEEE/RSJ International Conference on Intelligent Robots and Systems, 2015, pp. 3346–3351.

[17] M. Neunert, M. Stäuble, M. Giftthaler, C. D. Bellicoso, J. Carius, C. Gehring, M. Hutter, J. Buchli, Whole-body nonlinear model predictive control through contacts for quadrupeds, IEEE Robotics and Automation Letters 3 (3) (2018) 1458–1465.
[18] Y. Tassa, T. Erez, E. Todorov, Synthesis and stabilization of complex behaviors through online trajectory optimization, in: 2012 IEEE/RSJ International Conference on Intelligent Robots and Systems, 2012, pp. 4906–4913.
[19] Q. Bombled, O. Verlinden, Indirect foot force measurement for obstacle detection in legged locomotion, Mechanism and Machine Theory 57 (2012) 40–50.
[20] L. Mao, F. Gao, Y. Tian, Y. Zhao, Novel method for preventing shin-collisions in six-legged robots by utilising a robot–terrain interference model, Mechanism and Machine Theory 151 (2020).
[21] M. A. Hopkins, D. W. Hong, A. Leonessa, Compliant locomotion using whole-body control and divergent component of motion tracking, in: 2015 IEEE International Conference on Robotics and Automation, 2015, pp. 5726–5733.
[22] G. Bledt, P. M. Wensing, S. Ingersoll, S. Kim, Contact model fusion for event-based locomotion in unstructured terrains, in: 2018 IEEE International Conference on Robotics and Automation, 2018, pp. 4399–4406.
[23] H. Lee, Y. Lee, J. Park, Contact-consistent disturbance observer for floating-base robots, in: International Symposium on Experimental Robotics, 2018, pp. 475–484.
[24] N. Dini, V. J. Majd, Sliding-mode tracking control of a walking quadruped robot with a push recovery algorithm using a nonlinear disturbance observer as a virtual force sensor, Iranian Journal of Science and Technology, Transactions of Electrical Engineering (2019) 1–25.
[25] F. Ruggiero, J. Cacace, H. Sadeghian, V. Lippiello, Passivity-based control of vtol uavs with a momentum-based estimator of external wrench and unmodeled dynamics, Robotics and Autonomous Systems 72 (2015) 139–151.
[26] C. Ott, M. A. Roa, G. Hirzinger, Posture and balance control for biped robots based on contact force optimization, in: 2011 11th IEEE-RAS International Conference on Humanoid Robots, IEEE, 2011, pp. 26–33.
[27] B. Henze, C. Ott, M. Roa, Posture and balance control for humanoid robots in multi-contact scenarios based on model predictive control, in: 2014 IEEE/RSJ International Conference on Intelligent Robots and Systems, 2014, pp. 3253–3258.
[28] J. Di Carlo, P. M. Wensing, B. Katz, G. Bledt, S. Kim, Dynamic locomotion in the mit cheetah 3 through convex model-predictive control, in: 2018 IEEE/RSJ International Conference on Intelligent Robots and Systems, 2018, pp. 1–9.
[29] B. Henze, M. A. Roa, C. Ott, Passivity-based whole-body balancing for torque-controlled humanoid robots in multi-contact scenarios, The International Journal of Robotics Research 35 (12) (2016) 1522–1543.
[30] B. Siciliano, L. Sciavicco, L. Villani, G. Oriolo, Robotics: modelling, planning and control, Springer, 2010.
[31] Z. Li, S. Ge, S. Liu, Contact-force distribution optimization and control for quadruped robots using both gradient and adaptive neural networks, IEEE Transactions on Neural Networks and Learning Systems 25 (8) (2013) 1460–1473.
[32] Z. Cong, A. Honglei, C. Wu, L. Lang, Q. Wei, M. Hongxu, Contact force estimation method of legged-robot and its application in impedance control, IEEE Access 8 (2020) 161175–161187.
[33] X. Zeng, S. Zhang, H. Zhang, X. Li, H. Zhou, Y. Fu, Leg trajectory planning for quadruped robots with high-speed trot gait, Applied Sciences 9 (7) (2019).
[34] M. Mistry, L. Righetti, Operational space control of constrained and underactuated systems, Robotics: Science and systems VII (2012) 225–232.
[35] F. Aghili, A unified approach for inverse and direct dynamics of constrained multibody systems based on linear projection operator: Applications to control and simulation, IEEE Transactions on Robotics 21 (5) (2005) 834–849.
[36] L. Righetti, J. Buchli, M. Mistry, S. Schaal, Inverse dynamics control of floating-base robots with external constraints: A unified view, in: 2011 IEEE International Conference on Robotics and Automation, 2011, pp. 1085–1090.
[37] A. W. Winkler, D. C. Bellicoso, M. Hutter, J. Buchli, Gait and trajectory optimization for legged systems through phase-based end-effector parameterization, IEEE Robotics and Automation Letters 3 (2018) 1560–1567.

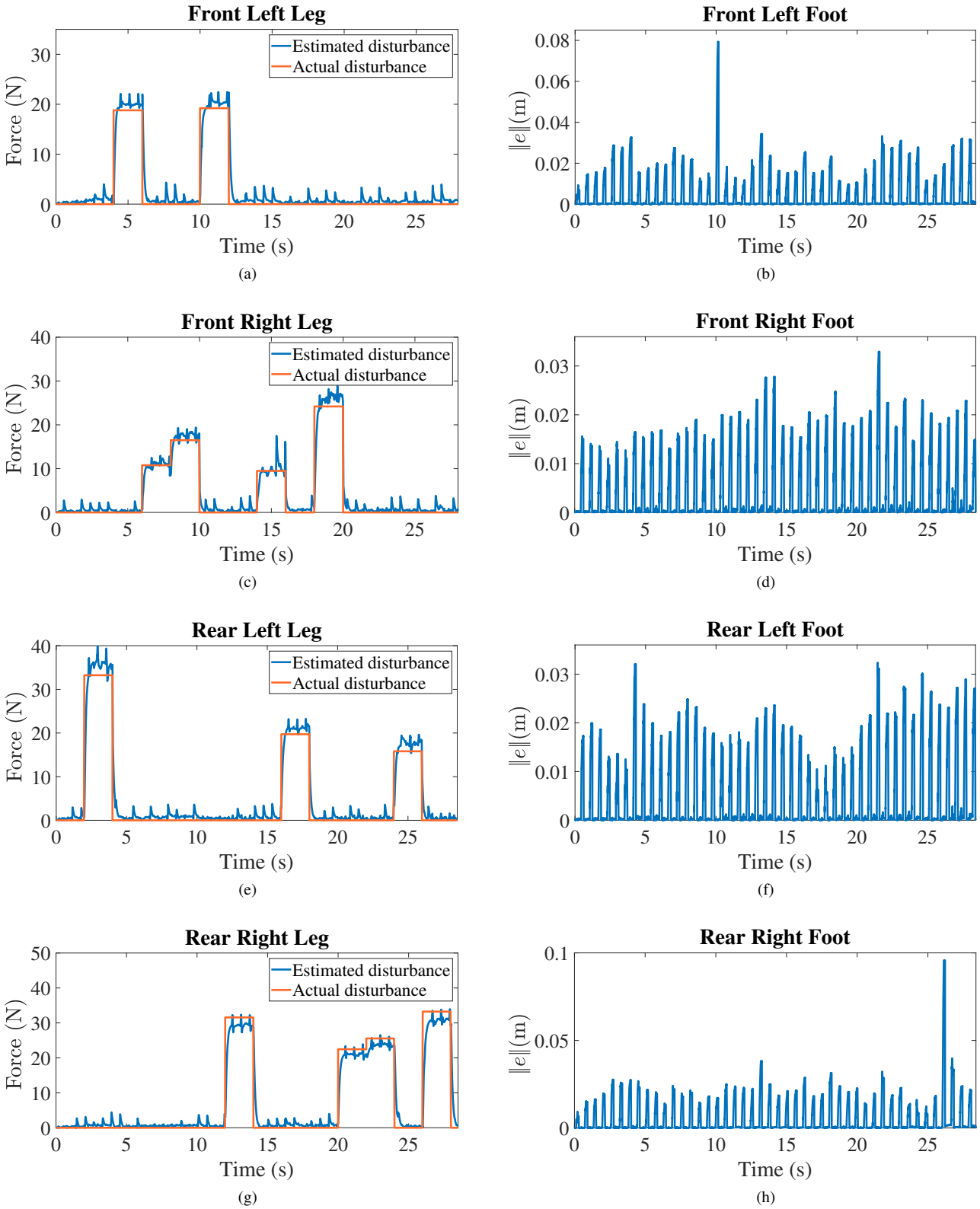

Figure 13: Case Study 4-Ideal situation. (a),(c),(e),(g) Estimation of the disturbance on the four legs, in blue the estimated force, in orange the actual force. (b),(d),(f),(h) Error norm of respective feet.

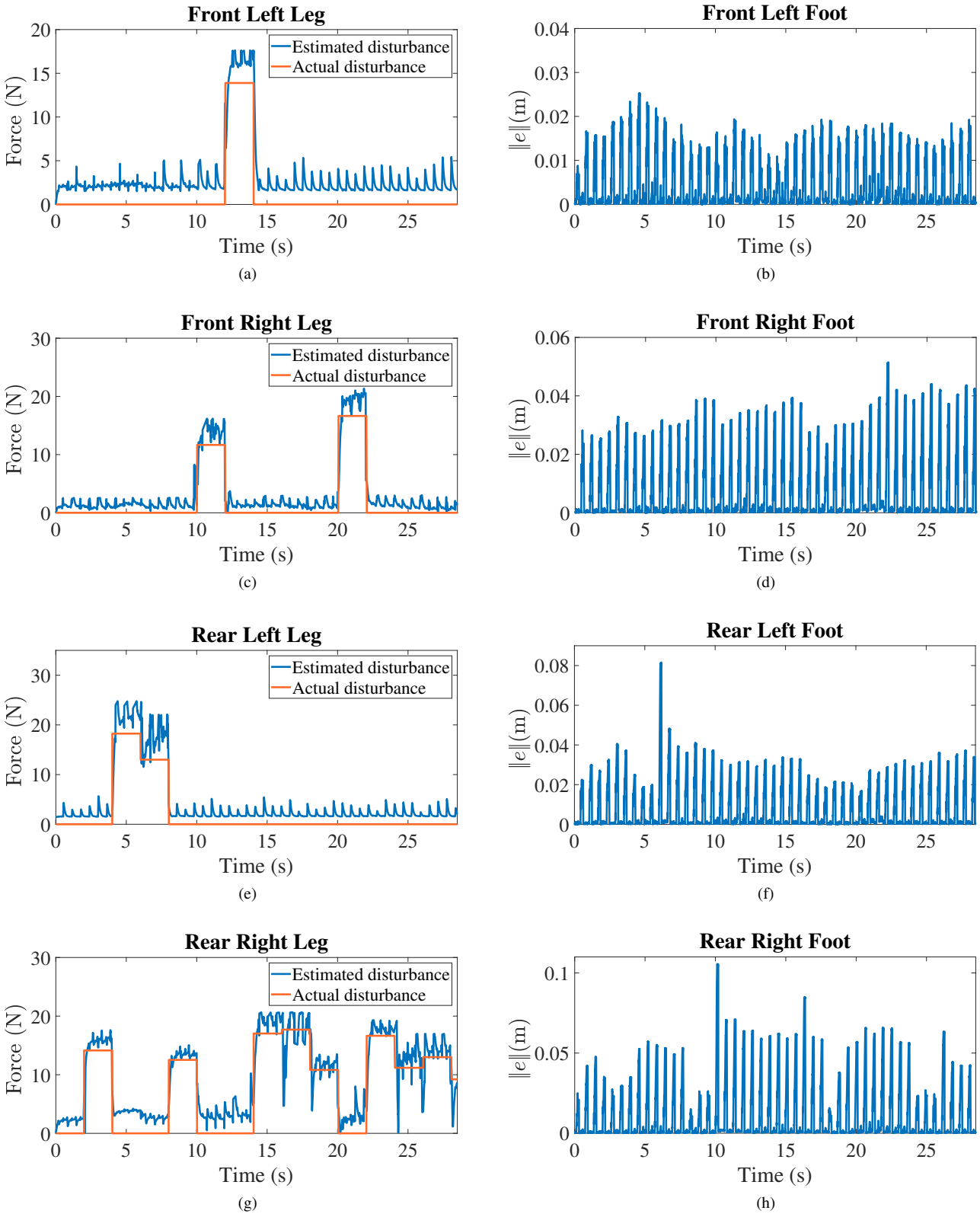

Figure 14: Case Study 4-White Gaussian noise added on the joint torque measurement. (a),(c),(e),(g) Estimation of the disturbance on the four legs, in blue the estimated force, in orange the actual force. (b),(d),(f),(h) Error norm of respective feet.

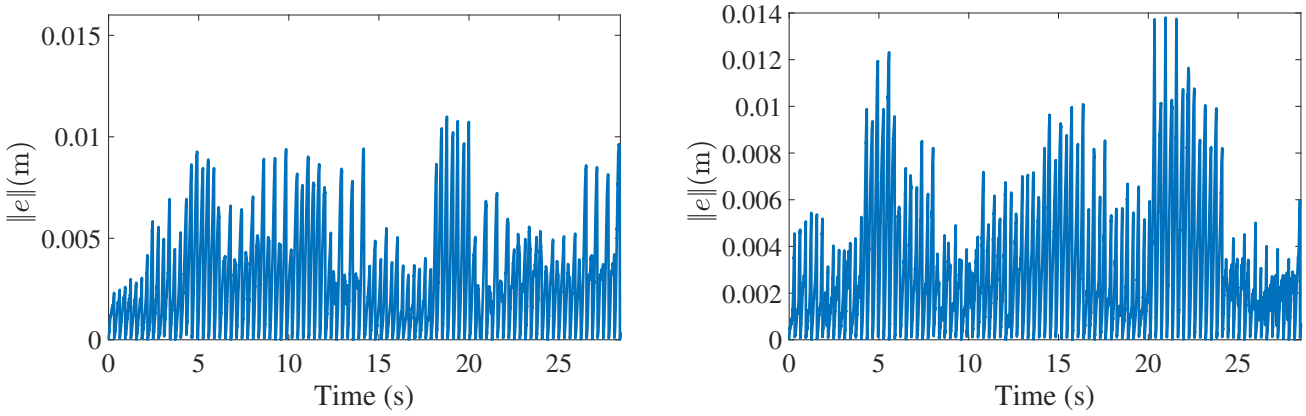

Figure 15: Case Study 4: Error norm of the robot's CoM using the proposed whole-body controller. (a) Ideal situation. (b) White Gaussian noise added on the joint torque measurement.

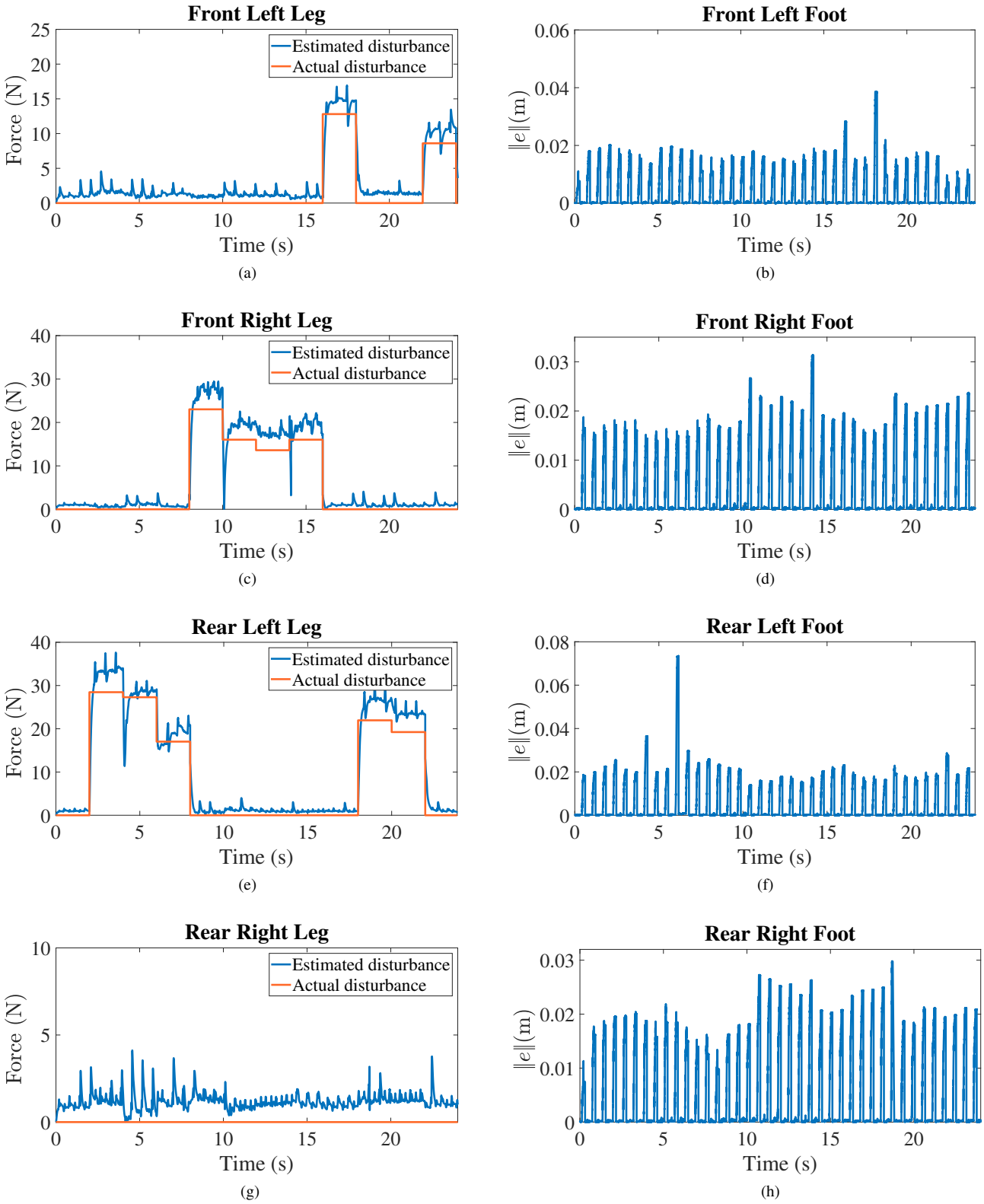

Figure 16: Case Study 5. (a),(c),(e),(g) Estimation of the disturbance on the four legs, in blue the estimated force, in orange the actual force. (b),(d),(f),(h) Error norm of respective feet.

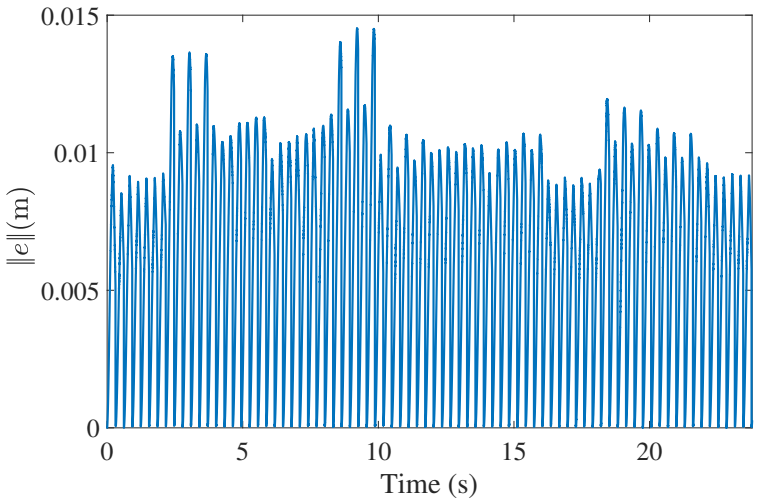

Figure 17: Case Study 5: Error norm of the robot's CoM using the proposed whole-body controller.

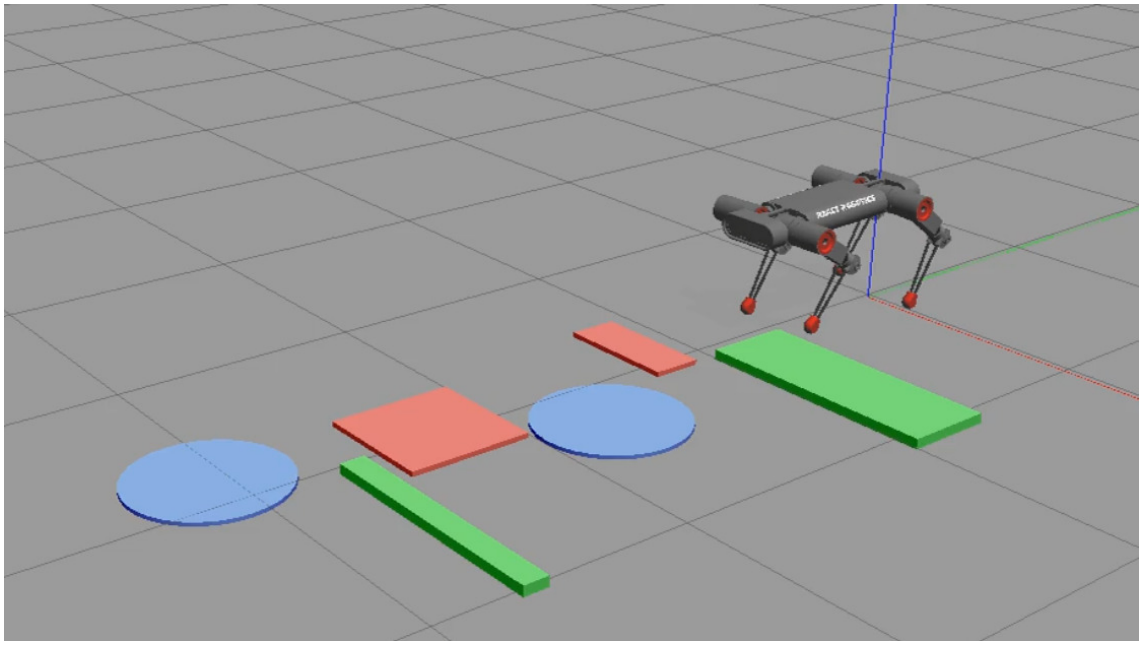

Figure 18: Case Study 6: Environment of the Case Study 6. The friction coefficient is: 0.4 for blue blocks, 0.6 for green blocks, 0.8 for red blocks, and 1 for the ground. The height of the blocks is: 0.015 m for blue blocks, 0.04 m for green blocks, and 0.02 m for red blocks.

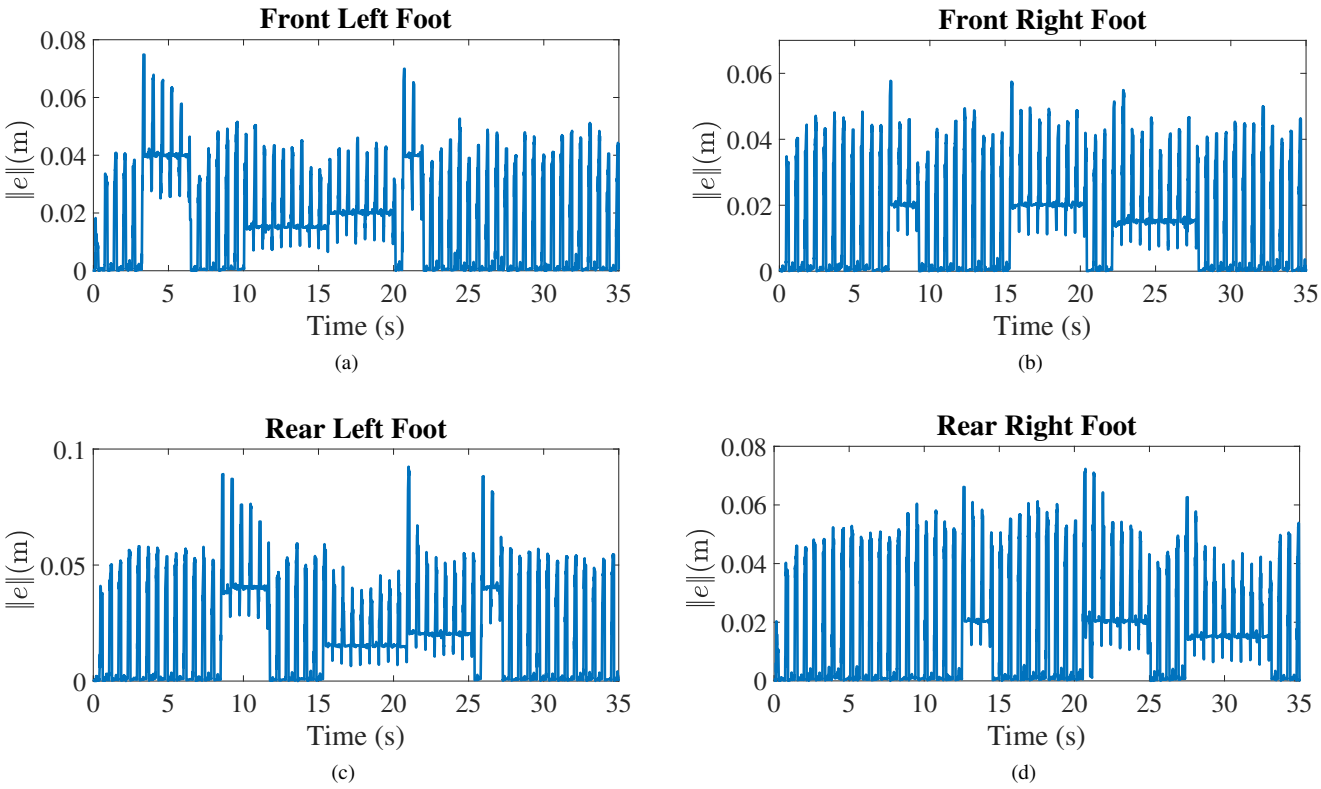

Figure 19: Case Study 6. Error norm of the feet.

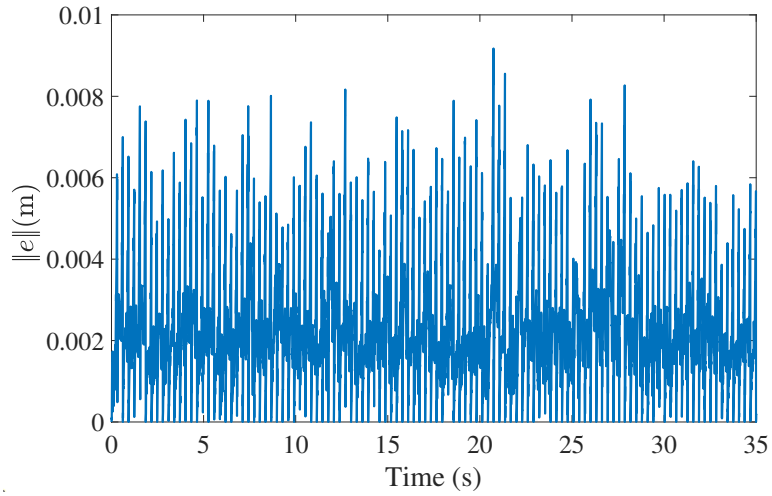

Figure 20: Case Study 6: Error norm of the robot's CoM using the proposed whole-body controller.